

Ideal Registration? Segmentation is All You Need

Xiang Chen¹, Fengting Zhang¹, Qinghao Liu¹, Min Liu^{1*}, Kun Wu², Yaonan Wang¹, Hang Zhang³

¹Hunan University, ²Shanghai Normal University, ³Cornell University

Abstract

Deep learning has revolutionized image registration by its ability to handle diverse tasks while achieving significant speed advantages over conventional approaches. Current approaches, however, often employ globally uniform smoothness constraints that fail to accommodate the complex, regionally varying deformations characteristic of anatomical motion. To address this limitation, we propose **SegReg**, a **Segmentation-driven Registration** framework that implements anatomically adaptive regularization by exploiting region-specific deformation patterns. Our SegReg first decomposes input moving and fixed images into anatomically coherent subregions through segmentation. These localized domains are then processed by the same registration backbone to compute optimized partial deformation fields, which are subsequently integrated into a global deformation field. SegReg achieves near-perfect structural alignment (98.23% Dice on critical anatomies) using ground-truth segmentation, and outperforms existing methods by 2-12% across three clinical registration scenarios (cardiac, abdominal, and lung images) even with automatic segmentation. Our SegReg demonstrates a near-linear dependence of registration accuracy on segmentation quality, transforming the registration challenge into a segmentation problem. The source code will be released upon manuscript acceptance.

Introduction

Deformable image registration is a fundamental task for various medical imaging tasks such as surgical planning, surgical navigation, disease diagnosis and motion analysis (Chen et al. 2021a; Viergever et al. 2016), which aims to establish dense, non-linear correspondences (deformation fields) between the moving and fixed images.

Traditional methods (Beg et al. 2005; Ashburner 2007; Vercauteren et al. 2009; Avants et al. 2011; Marstal et al. 2016) typically employ a multi-step optimization strategy aimed at minimizing an error function comprising similarity and smoothness regularization. The similarity metric quantifies the discrepancy between the warped moving image and the fixed image, whereas smoothness regularization enforces a smooth deformation field, thereby mitigating irregular motions. Although these methods are reliable for accurate registration, their time-intensive process is a notable limitation in scenarios demanding rapid registration (Chen et al. 2021a).

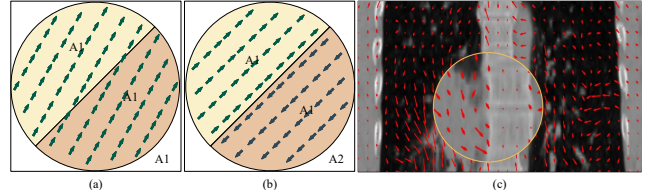


Figure 1: Visualization of different motion assumptions. Most learning-based registration methods assume totally smooth deformation fields (Assumption A1). Instead, SegReg assumes deformation fields to be smooth within each sub-region while discontinuous on the boundaries (Assumption A2), accommodating more complex scenarios like (c).

Deep learning registration methods have seen broad application, offering efficient, near-real-time registration post-training(Balakrishnan et al. 2019; Chen et al. 2022). Unsupervised registration networks(Balakrishnan et al. 2019), which utilize solely the moving and fixed images as inputs, have matched the performance of conventional approaches. They typically employ similarity metrics such as Mean Squared Error (MSE) and Normalized Cross Correlation (NCC), coupled with smooth regularization techniques like L2 diffusion, for network training. To enhance registration performance, weakly supervised registration networks incorporate supplementary segmentation masks or landmarks as additional loss functions like Dice loss to refine the guidance cite chen2021deepDiscontinuity. Despite the escalating complexity of registration models in recent years, notably with the incorporation of transformers (Chen et al. 2022), large convolutional kernels (Jia et al. 2022) and pyramid-based registration (Zhang et al. 2024a; Wang, Ni, and Wang 2024), the enhancements in registration accuracy have reached a plateau. In addition, (Jena et al. 2024) points out that, architectural designs in learning-based methods are unlikely to affect the registration performance, without the guidance of weak supervision information. Therefore, additional label information is imperative to unlock the full potential of learning-based approaches and realize substantial advancements in the precision of registration techniques.

To our analysis, a primary constraint on current registration accuracy is the smooth regularization inherent in most deep learning-based registration networks (Balakrishnan et al. 2019; Chen et al. 2022), which assumes **the de-**

*Corresponding authors:liu_min@hnu.edu.cn

formation fields are globally smooth (Assumption A1). While valid for simple tasks (e.g., single-object alignment or local minor physiological shifts), this paradigm artificially constrains performance in anatomically heterogeneous scenarios due to overly constrained regularization. As shown in Figure 1, scenarios (a) and local regions in (b) and (c) align with Assumption A1, whereas the complete images of (b) and (c) do not. In medical imaging, the diverse properties and motions of organs and tissues are poorly captured by global smooth regularization, which hinders the accurate alignment of disparate organs or tissues. To better approximate realistic motion and enhance registration performance, discontinuity-preserving registration techniques (Ng and Ebrahimi 2020; Chen et al. 2021b) are necessary, which assumes **the deformation fields to be locally smooth and globally discontinued (Assumption A2)**, achieved via structure guidance.

Contrary to registration, segmentation ground truth (GT) is more accessible, with numerous public segmentation models available (Wasserthal et al. 2023; Isensee et al. 2021). Despite scanner and scanning condition variations, images of identical organs and modalities share a high degree of similarity. Consequently, with limited local data, high segmentation accuracy can be attained by finetuning these public segmentation models. The emergence of nnUNet (Isensee et al. 2021) and Segment Anything Model (SAM) (Kirillov et al. 2023; Chen et al. 2024a; Huang et al. 2024)) has streamlined effective segmentation across diverse tasks, even with limited training data. Building on these strategies, enhancing registration performance through precise segmentation seems a logical next step.

In this paper, we embrace the principles of discontinuity-preserving registration (**Assumption A2**), assuming: (1) the motion within organs/regions is smooth and consistent in the absence of external factors, and (2) motion between different organs/regions could be either continuous or discontinuous, where the discontinuity occurs at the boundaries between different organs/regions. This assumption, while simple, encompasses a wider range of motion patterns than the traditional uniform smoothness assumption. Leveraging this, optimal registration within each sub-region is achievable through a simple end-to-end network under **Assumption A1**. We introduce SegReg, a novel framework that transforms registration into a segmentation task, comprising region-wise mapping and deformation field composition. Region-wise mapping aligns corresponding subregions in moving and fixed images, while composition integrates subregional deformation fields into a complete image field. Although the composition scheme naturally captures discontinuities, it may sometimes overemphasize boundary discontinuities. To ensure smooth transitions between subregions, we further employ an Euclidean distance transform (EDT) loss in addition to the standard Dice loss. The contributions are summarized as follows:

- We propose a novel registration framework, SegReg, which transfers the complex registration problem into a couple of simple region-wise registrations, via segmentation, naturally preserving discontinuities and breaking the upper limit of current registration approaches.

- We introduce EDT loss, which employs different weights for segmentation masks within each region, enabling a smoother transfer across region boundaries while keeping discontinuity.
- Results on three different registration tasks demonstrate that the proposed SegReg framework significantly outperforms other state-of-the-art (SOTA) methods.

Related Work

Supervised Registration Methods

Unlike other visual tasks, image registration lacks definitive GT deformations. Given the inaccessibility of true deformation fields, early deep registration methods relied on synthetic deformations or those predicted by traditional approaches. Supervised methods train end-to-end networks to predict deformation fields by minimizing the discrepancy between predictions and reference deformations. For instance, similarity-steered regression (Cao et al. 2017) uses SyN (Avants et al. 2008) and Diffeomorphic Demons (Vercauteren et al. 2009) to generate GT deformation fields. Similarly, BIRNet (Fan et al. 2019) uses existing methods' deformations and trains the network alongside intensity dissimilarity measure. SVF-Net (Rohé et al. 2017) constructs target fields by matching shapes (Durrleman et al. 2014) from segmentations. In addition, synthetic transformations, including affine and elastic deformations (Eppenhof and Pluim 2018; Young et al. 2022), are integrated and composed across scales to create GT fields.

Unsupervised Registration Methods

For unsupervised registration, the available data for network training are only the input images. To train the network, an end-to-end network takes moving and fixed images as input and predicts a corresponding deformation field. A spatial transformer block warps moving images to approach fixed images. The training loss comprises two parts: the similarity between warped moving image and fixed image, and the smooth regularisation of deformation fields. VoxelMorph (Balakrishnan et al. 2019; Dalca et al. 2019) led the way in unsupervised registration, showing a learning-based method can match traditional iterative methods' results in under a second for volumetric brain scans. Subsequently, numerous networks have been developed to enhance the accuracy of registration, smoothness of deformation fields or computational efficiency. In architecture design, studies have investigated parallel (Kang et al. 2022; Jia et al. 2022) and cascaded structures (Zhao et al. 2019; Mok and Chung 2020b), attention-based transformers (Chen et al. 2022; Shi et al. 2022) along with multi-layer perceptrons (Meng et al. 2024) for enhanced learning. For enhancing computational efficiency, DeepFlash (Wang and Zhang 2020) and Fourier-Net (Jia et al. 2023a,b) approximate the full deformation field with a band-limited version, while approaches such as LessNet (Jia et al. 2024) with a decoder-only configuration and the Slicer Network (Zhang et al. 2024b) with an encoder-only setup reduce redundancy and boost efficiency.

Weakly-supervised Registration

Weakly-supervised registration research incorporates additional supervision, such as segmentation masks or landmarks, in network training, falling into two categories: (1) using this information solely during training, and (2) employing it in both training and testing phases. The first approach often integrates these cues as an auxiliary similarity loss, like Dice loss (Zhang et al. 2024a), enhancing unsupervised networks via weakly-supervised training and boosting registration precision. Notable developments include novel loss functions that impose local-oriented consistency (Mok and Chung 2020a) for diffeomorphism (Dalca et al. 2019), auxiliary segmentation for anatomical alignment (Balakrishnan et al. 2019; Mok and Chung 2021), and regularizers for curvature (Hering et al. 2021) and keypoints (Hering et al. 2021; Zhang et al. 2024b). The second approach, exemplified by DDIR (Chen et al. 2021b), constructs a multi-channel encoder-decoder for cardiac registration, leveraging segmentation masks to segment the image into distinct pairs, left ventricle blood pool (LVPB), left ventricle myocardium (LVM), right ventricle (RV) and background, respectively, and conducting region-wise registration. Similarly, Chen et al. (Chen et al. 2024b) utilized fixed image segmentation and a text-encoder from large language models to create a spatially covariant filter, showing that even low-accuracy automatic segmentation can significantly enhance registration.

Due to limited labelled data, previous research has often avoided integrating segmentation into registration networks. Despite using weakly-supervised training, segmentation was typically used only for Dice loss, bypassing its need during inference. These approaches, lacking labelled guidance in the inference, hindered the achievement of discontinuity-preserving registration and restricted registration accuracy. With the progress in public segmentation models and foundation segmentation models, accurate segmentation has become more feasible. Our SegReg bridges segmentation and registration, surpassing current registration accuracy limits.

Methodology

Framework of SegReg

The overall framework of SegReg is depicted in Figure 2. The core concept of SegReg is to match the moving image and fixed image by aligning each local region. For this process, segmentation masks are essential, which can be sourced from either manual annotations or automated segmentation techniques. Automated segmentation masks can be derived from the same dataset used for network training or by finetuning a pre-existing segmentation model, such as SAM. Each local pair's deformation is calculated by a registration backbone, yielding sub-deformation fields that correspond to individual sub-regions. During training, we randomly select pairs of regions from the original moving and fixed images, training the registration backbone in a manner akin to a standard weakly-supervised registration network. In the inference, all pairs of regions are processed by the registration backbone to predict sub-deformation fields, which are then composed into overall deformation fields.

The warped image is subsequently generated by applying overall deformation fields to the original moving images.

Denote the moving image as I_m and fixed image as I_f , the process of image registration can be formulated as,

$$\Phi(x) = x + \mathbf{u}(x), \quad (1)$$

$$I_f = \Phi(x) \circ I_m, \quad (2)$$

where the $\mathbf{u}(x)$ is the displacement field, denoting the movement (x,y for 2D image registration, and x,y,z for 3D image registration) of each voxel in the images. The $\Phi()$ is the warping function from the moving image to the fixed image. For n-label images, denote the moving and fixed segmentation masks as S_m and S_f , then $S_m = \{S_m^0, \dots, S_m^{n-1}\}$, $S_f = \{S_f^0, \dots, S_f^{n-1}\}$. Within each sub-region, the deformation field is smooth. In the training, we can rewrite the formula 2 for i-th region as,

$$I_f \times S_f^i = \Phi_i(x) \circ (I_m \times S_m^i), i \in \{0, \dots, n-1\}. \quad (3)$$

Registration Backbone

To demonstrate the efficiency of our proposed SegReg framework, we choose a simple UNet as the registration backbone, following (Balakrishnan et al. 2019; Dalca et al. 2019; Chen et al. 2021b). As shown in Figure 3, the registration backbone comprises an encoder and a decoder. The encoder consists of four layers that successively downsample the input images by half with each layer. The decoder, mirroring the encoder, comprises four layers that upsample the feature maps to double their original size. Skip-connection is applied on the corresponding layers in the encoder and decoder. The moving and fixed regions are concatenated at the beginning, and then fed into the encoder-decoder to predict the velocity field \mathbf{v} . The deformation fields \mathbf{u} are obtained by integration from the velocity fields \mathbf{v} , following (Dalca et al. 2019). Note that, under our SegReg framework, even a simple UNet is enough to obtain superior registration accuracy, while it can also be replaced by more efficient or powerful architectures, to further improve registration performance.

Deformation Field Composition

Given that motion within a sub-region is smooth, a straightforward registration backbone that adheres to Assumption A1 can effectively predict deformation within each sub-region. Nevertheless, this strategy introduces a challenge: the derived deformation fields are localized and do not account for the global deformation. Consequently, in the testing, a composition scheme is required to integrate the sub-deformation fields from each region into complete deformation fields. Denote the deformation field corresponding to segmentation mask i as: Φ_i , the deformation field composition process is formulated as $\Phi(x) = \sum_i^n (\Phi_i(x)) \times S_i$. Once achieving the Φ , the final warped images are achieved by warping moving images with Φ .

The split-and-merge strategy offers two key advantages: (1) By aligning corresponding local regions in isolation, we can capture the optimal smooth registration within each sub-region, leveraging the inherent continuity of motion within localized areas. (2) The amalgamation of these smooth sub-deformation fields into complete deformation fields ensures

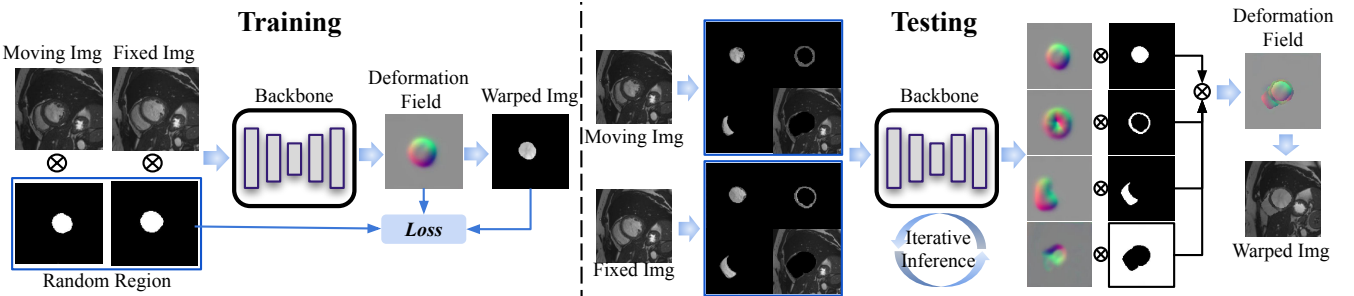


Figure 2: Schema of SegReg. The input moving and fixed images are first split into different pairs of interest using the segmentation masks. In the training process, a random pair is fed into the registration backbone at each iteration, and update the parameters of the registration backbone via back-propagation. In the test phase, all pairs of interest are fed into the registration backbone and predict the corresponding sub-deformation fields, and then combined to obtain the final deformation fields.

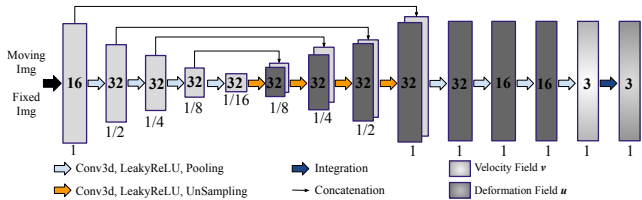


Figure 3: Architecture of registration backbone in SegReg. For simplicity, we utilize a general UNet as the backbone.

that the final deformation is locally smooth while global discontinuities. This naturally aligns with the principles of discontinuity-preserving registration, effectively accommodating varying motion patterns across different regions.

Loss Function

To optimize our SegReg, we employ a hybrid loss function strategy that integrates two components: a similarity loss and a regularization loss. The similarity loss is designed to assess and quantify the alignment between the warped moving image and the fixed image. On the other hand, the regularization loss is instrumental in enforcing the smoothness of the predicted deformation fields, which is crucial for ensuring the physiological plausibility of the transformations.

The similarity loss further comprises two parts, a voxel-wise loss L_v and a mask-wise loss L_m . The voxel-wise loss can be NCC or MSE loss. Regarding the mask-wise loss, a popular choice could be the Dice loss, which helps to align the images according to regions and improve registration accuracy. However, in the SegReg framework, it may cause severe gradient mutation across the boundaries, leading to significant discontinuity on the boundary. To alleviate the phenomenon, we further propose an EDT loss which transfers the original binary segmentation masks (in training, the input registration pair only contains the foreground and background) into EDT masks, as shown in Figure 4. Different from binary masks, the pixels/voxels in the foreground turn to their distance to the boundaries (normalized to 0-1), thereby implying different weights to pixels/voxels and surpassing those pixels/voxels on the boundary. Then the EDT loss is computed as the MSE loss between the warped mov-

ing EDT masks and fixed EDT masks, formulated as,

$$L_{edt} = \sqrt{(EDT_f - \Phi_i(x) \circ EDT_m)^2}. \quad (4)$$

According to our assumption, the deformation fields are smooth and continuous within each sub-region. In the training phase, we only register one pair of regions each iteration. Following previous research (Dalca et al. 2019; Balakrishnan et al. 2019), we directly choose L_2 -regularisation on each deformation field as the smooth regularisation R . Therefore, the total loss L_{total} is formulated as,

$$L_{total} = \gamma_0 \times L_v + \gamma_1 \times L_m + \gamma_2 \times R, \quad (5)$$

where the $\gamma_0, \gamma_1, \gamma_2$ are hyperparameters to balance the similarity loss and regularisation, set empirically.

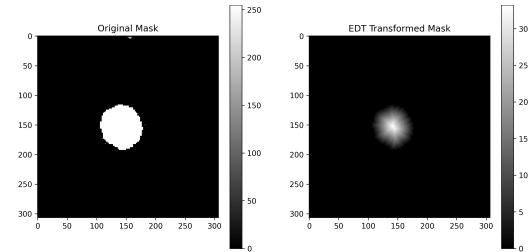


Figure 4: Segmentation mask and corresponding EDT mask.

Training and Inference

The SegReg framework's adaptability enables its utilization in dual capacities: as a learning-based registration network or as an iterative registration technique, mirroring conventional approaches. For learning-based registration, the registration pair is initially segmented into various regions of interest, guided by the segmentation masks. During training, SegReg randomly introduces a random pair of local regions into the registration backbone at each iteration. In the inference, every pair of regions identified by the segmentation masks is fed to the registration backbone to generate corresponding sub-deformation fields, which are then combined by a composition operation to yield the complete deformation fields. The warped image is obtained by applying the

complete deformation field to the original moving images, thus facilitating precise alignment with fixed images.

For iterative registration, SegReg is similar to traditional iterative registration methods, which register the moving and fixed images via multiple iterations and do not require a training stage prior to the inference. Within each iteration, the deformation fields are refined based on a hybrid loss function that encompasses both similarity metrics and smooth regularization. Instead of using global smooth regularization, we compute the summary of L_2 -regularization within each sub-region (split by the corresponding fixed segmentation) as the total smooth regularization R .

Experiments & Results

Datasets and Implementation Details

We demonstrate our SegReg framework on both computed tomography (CT) and magnetic resonance (MR) image modalities, with inter-subject and intra-subject settings. Specifically, we use the ACDC dataset (Bernard et al. 2018) for intra-subject cardiac cine-MR image registration, the Abdomen CT dataset for inter-subject registration (Xu et al. 2016), and ThroaxCBCT dataset (Hugo et al. 2017) for intra-subject multi-modality thorax image registration. More details about the datasets can be found in the Appendix.

In our experiments, all models were developed using PyTorch library in Python on an A6000 GPU machine. We utilize Adam optimizer for network training, with an initial learning rate of $1e - 4$ and a polynomial learning rate scheduler with a decay rate of 0.9. MSE loss, NCC loss, and MSE loss on MIND features (Heinrich et al. 2012) are used as the voxel-wise loss L_v in cardiac images, abdomen images, and thorax images, respectively. We build three versions of SegReg, SegReg-Dice, SegReg-EDT and SegReg-EDT&Dice, using Dice loss, EDT loss and the hybrid loss of them ($L_m = (L_{Dice} + 100 \times L_{EDT})/2$) as the mask-wise loss L_m in network training. In cardiac image registration, we set $\gamma_0 : \gamma_1 : \gamma_2 = 1 : 0.1 : 0.01$ for SegReg-Dice and SegReg-EDT&Dice, and $\gamma_0 : \gamma_1 : \gamma_2 = 1 : 10 : 0.01$ for SegReg-EDT. In abdominal image registration, we choose $\gamma_0 : \gamma_1 : \gamma_2 = 1 : 1 : 0.1$ for SegReg-Dice and SegReg-EDT&Dice, $\gamma_0 : \gamma_1 : \gamma_2 = 1 : 100 : 0.1$ for SegReg-EDT.

We compare our SegReg framework with SOTA learning-based registration models. All the approaches are trained in a weakly-supervised manner, trained with Dice loss. For a fair comparison, we employ two publicly available segmentation models: Swin-UNETR (Tang et al. 2022; Hatamizadeh et al. 2022) and nnUNet (Isensee et al. 2021), to segment abdominal CT images and cardiac MR images, respectively, and then feed the resultant predictions into our SegReg for inference. We utilize their pre-trained models directly from online sources, **without any local fine-tuning**. The segmentation accuracy on the abdominal and ACDC test sets are 75.83% and 91.19%, respectively. For ThoraxCBCT, we obtain results directly from the public leaderboard.

Following previous research (Balakrishnan et al. 2019) and challenge protocols (Hering et al. 2022), we evaluate anatomical alignment using the Dice Similarity Coefficient (Dice) and the 95% Hausdorff Distance (HD95). To assess

Model	Dice (%) \uparrow	HD95 (mm) \downarrow	SDlogJ \downarrow	J(<0) \downarrow	MA _s (G) \downarrow	PS (MB) \downarrow
Initial	58.14	11.95	-	-	-	-
VoxelMorph (Balakrishnan et al. 2018)	81.95	7.18	0.07	0.00	19.57	0.33
TransMorph (Chen et al. 2022)	82.75	6.98	0.084	249.62	54.34	46.69
LKU-Net (Jia et al. 2022)	82.37	6.66	0.08	0.00	160.58	33.35
Fourier-Net (Jia et al. 2023a)	83.98	6.41	0.07	1.12	86.11	17.43
MemWarp (Zhang et al. 2024a)	87.81	5.36	0.08	50.96	1267.28	47.78
RDP (Wang, Ni, and Wang 2024)	85.99	6.55	0.086	0.00	154.14	8.92
DDIR (Chen et al. 2021b)	88.03	9.91	0.121	45.68	78.19	1.31
SegReg-Dice(Ours)	89.98	5.08	0.36	41.52	19.57	0.33
SegReg-EDT(Ours)	87.79	6.03	0.09	0.36	19.57	0.33
SegReg-EDT&Dice(Ours)	89.24	5.45	0.15	6.68	19.57	0.33

Table 1: Quantitative comparison on the cardiac ACDC dataset. Best-performing metrics are highlighted in bold. Symbols indicate direction: \uparrow for higher is better, \downarrow for lower is better. “Initial” refers to results before registration.

Model	Dice (%) \uparrow	HD95 (mm) \downarrow	SDlogJ \downarrow
Initial	30.86	29.77	-
VoxelMorph (Balakrishnan et al. 2018)	47.05	23.08	0.13
TransMorph (Chen et al. 2022)	47.94	21.53	0.13
LKU-Net (Jia et al. 2022)	52.78	20.56	0.98
Xmorpher (Shi et al. 2022)	40.67	23.77	0.14
LapIRN (Mok and Chung 2020b)	54.55	20.52	1.73
Fourier-Net (Jia et al. 2023a)	42.80	22.95	0.13
ConvexAdam (Siebert, Hansen, and Heinrich 2021)	51.10	23.14	0.11
SAMConvex (Li et al. 2023)	53.65	18.66	0.12
RDP (Wang, Ni, and Wang 2024)	58.77	20.07	0.22
MemWarp (Zhang et al. 2024a)	60.24	19.84	0.53
textSCF (Chen et al. 2024b)	60.75	22.44	0.87
SegReg-Dice(Ours)	68.02	20.77	0.58
SegReg-EDT (Ours)	67.19	21.04	0.52
SegReg-EDT&Dice (Ours)	67.74	21.73	0.60

Table 2: Quantitative comparison on abdomen CT dataset.

field smoothness, we measure the standard deviation and number of foldings of the logarithm of the Jacobian determinant (SDlogJ and J(<0)). Computational complexity is assessed in cardiac image registration, using the multiply-add operations (MA_s) and total parameter size (PS).

Results and Analysis

Intra-subject Registration on ACDC. We assess the intra-subject registration performance of SegReg on cardiac MR images from the ACDC dataset, as shown in Table 1 and Figure 5 (Boxplot can be found in the Appendix Figure A2). Leveraging their capacity to manage large deformations, pyramid-based methods MemWarp (Zhang et al. 2024a) and RDP (Wang, Ni, and Wang 2024) demonstrate superior performance over conventional single-resolution deformation field prediction approaches. While achieving significantly enhanced registration accuracy ($p < 0.05$), these methods incur prohibitively high computational overhead. As a discontinuity-preserving registration method also incorporating segmentation in the network, DDIR (Chen et al. 2021b) outperforms MemWarp (Zhang et al. 2024a) and RDP (Wang, Ni, and Wang 2024). Under SegReg framework, even a simple UNet registration backbone can outperform pyramid-based registration approaches. Our SegReg achieves superior registration accuracy compared to both MemWarp (Zhang et al. 2024a), RDP (Wang, Ni, and Wang 2024) and DDIR (Chen et al. 2021b), while maintaining network complexity comparable to VoxelMorph (Balakrishnan et al. 2018), demonstrating the superiority.

Inter-subject Registration on Abdomen Images. We also demonstrate the superior capability of our SegReg framework in managing much larger deformations through inter-subject abdominal CT registration, as quantitatively validated in Table 2. Consistent with findings on the ACDC

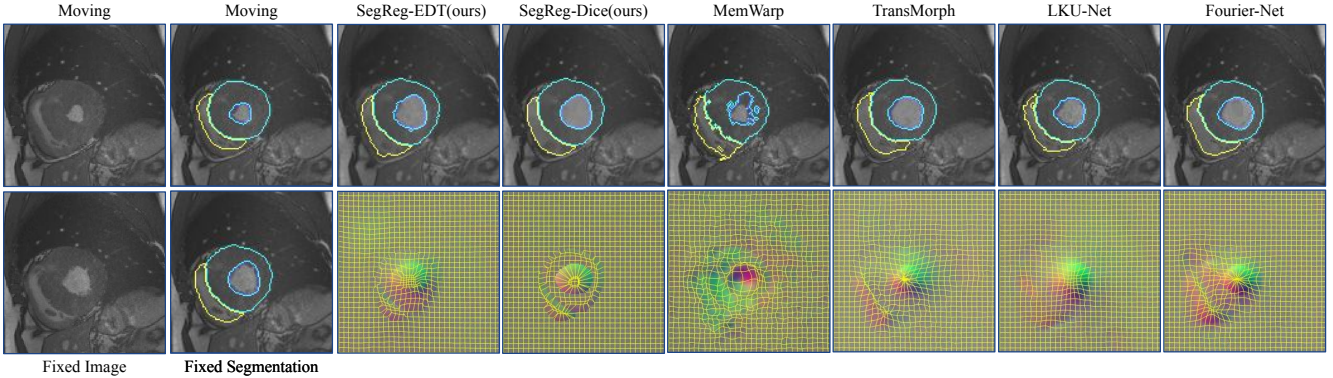


Figure 5: Qualitative comparison on ACDC. SegReg-Dice achieves the best alignment while the discontinuity is severe on the boundary. In contrast, the SegReg-EDT can achieve a good balance of registration accuracy and smoothness.

Model	Dice (%) \uparrow	HD95 (mm) \downarrow	SDlogJ \downarrow
Initial	58.14	11.95	-
VoxelMorph (Balakrishnan et al. 2018)	81.95	7.18	0.07
VoxelMorph-Img&Seg (GT) (Balakrishnan et al. 2018)	90.71	4.90	0.12
VoxelMorph-Seg (GT) (Balakrishnan et al. 2018)	91.32	3.74	0.08
SegReg-Dice(GT)	98.23	1.93	0.36
SegReg-EDT(GT)	95.44	3.62	0.08
SegReg-EDT&Dice(GT)	98.19	2.05	0.14
SegReg-Dice	89.98	5.08	0.36
SegReg-EDT	87.79	6.03	0.09
SegReg-EDT&Dice	89.24	5.45	0.15

Table 3: Quantitative comparison between automatic and GT segmentation on the cardiac ACDC dataset.

dataset, both MemWarp (Zhang et al. 2024a) and RDP (Wang, Ni, and Wang 2024) exhibit enhanced performance over conventional deep learning-based methods, attributable to their specialized design for large deformation scenarios. Notably, textSCF (Chen et al. 2024b), which similarly incorporates segmentation masks in its registration network, achieves competitive registration accuracy. Provided with equivalent segmentation inputs as textSCF (Chen et al. 2024b), our SegReg framework establishes new SOTA registration performance, attaining a mean Dice score of 68.02%. This represents a substantial improvement of approximately 12% over textSCF (Chen et al. 2024b), while simultaneously improving the smoothness of deformation fields.

Comparison Between Automatic and GT Segmentation. The presented SegReg performance is achieved using automated segmentation inputs with test Dice scores of 75.83% (abdominal CT) and 91.19% (ACDC). To further explore the theoretical upper bound, we implement SegReg with GT segmentation on ACDC (Table 3). We develop two VoxelMorph variants: VoxelMorph-Seg (segmentation-only input) and VoxelMorph-Img&Seg (image-segmentation concatenation). Comparative analysis reveals that integrating GT segmentation significantly enhances registration performance (about 10% Dice improvement), with segmentation-only inputs outperforming combined image-segmentation inputs in segmentation-based evaluation. Using automated segmentations, SegReg’s inherent capacity to preserve deformation field discontinuities enables comparable performance ($p > 0.05$) to both VoxelMorph variants (feeding GT segmentation). With GT segmentation inputs, SegReg surpasses both variants, achieving a mean Dice score exceeding

Model	Dice (%) \uparrow	HD95(mm)	SDlogJ \downarrow
Initial	31.3	55.358	-
deeds (Heinrich et al. 2013)	64.8	29.03	0.15
ConvexAdam (Siebert, Hansen, and Heinrich 2021)	56.8	45.22	0.16
ShiftMorph (Yang et al. 2024)	58.4	53.19	1.26
NiftyReg (Modat et al. 2010)	56.8	50.08	0.06
Fourier-Net (Jia et al. 2023a)	54.8	52.32	0.09
VoxelMorph++ (Heinrich and Hansen 2022)	50.3	28.56	0.13
SegReg (Ours)	68.9	13.94	0.30

Table 4: Quantitative comparison on the ThoraxCBCT dataset, derived directly from the online leaderboard.

95% (SegReg-Dice and SegReg-EDT&Dice are over 98%).

Iterative Registration on ThoraxCBCT. Our SegReg framework is not only confined to learning-based registration but can also be adapted for iterative registration akin to conventional methods, negating the need for pre-training before registration. We exemplify the application of SegReg in multi-modal intra-patient registration in ThoraxCBCT, where the goal is to align a subject’s fan-beam CT image with corresponding cone-beam CT images captured at the beginning and end of the therapy. Leveraging the online Totalsegmentor (D’Antonoli et al. 2024), we segment the input images into 13 distinct classes and proceed to align them regionally. As detailed in Table 4, SegReg achieves a markedly superior Dice score compared to other approaches. Notably, the HD score of SegReg is 13.94mm, approximately 15mm lower than suboptimal approach.

Discontinuity-preserving Analysis. The final deformation fields of SegReg are generated as a composite of multiple sub-deformation fields, inherently preserving discontinuities at the boundaries between disparate sub-regions. For each registration pair, the motion within each sub-region maintains smoothness, ensured by smooth regularization. This approach enables our SegReg to predict deformation fields that are smooth within each sub-region and discontinuous across different regions, effectively emulating realistic motion. A visualization of the motion vectors is presented in Figure 6. Discontinuities are evident in both SegReg-Dice and SegReg-EDT, in contrast to the results of VoxelMorph. Comparing SegReg-Dice and SegReg-EDT, the deformation field resulting from SegReg-EDT exhibits improved smoothness than that of SegReg-Dice.

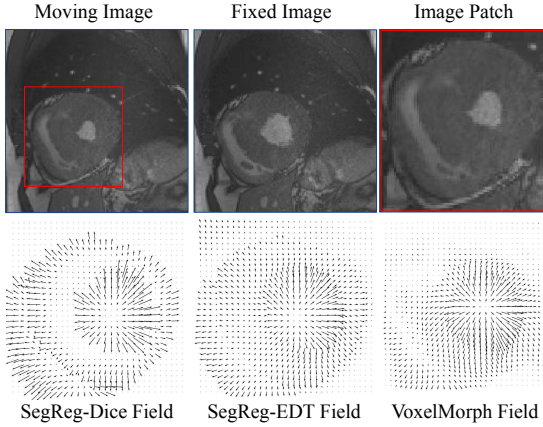


Figure 6: Visualisation of the motion vector from deformation of SegReg-Dice, SegReg-EDT and VoxelMorph.

How Segmentation Affects Registration? Given that SegReg primarily relies on segmentation to align the moving and fixed images, the quality of segmentation performance inherently sets an upper limit on the achievable registration accuracy. To investigate the impact of segmentation performance on registration accuracy, we train a nnUNet from scratch and employ the models at various training stages to generate segmentation masks with varying degrees of accuracy. Subsequently, we feed these different segmentations into SegReg and assess the resulting registration accuracy, as depicted in Figure 7. We observed that **SegReg’s registration accuracy shows a near-linear dependence on segmentation accuracy**. Although the registration accuracy of SegReg-EDT is slightly inferior to that of SegReg-Dice, it compensates by predicting smoother deformation fields. SegReg-EDT&Dice gradually achieves a balance between these two models with increasing segmentation accuracy. The registration accuracy only experiences a marginal decline relative to the segmentation accuracy, demonstrating the validity of our segmentation-driven registration framework in preserving anatomical consistency. This finding re-frames image registration as a segmentation-guided learning problem, where optimal correspondence is predicted automatically from precise tissue boundary delineation.

Influence of the Number of Segmentation Classes. To elucidate the impact of number of segmentation classes on registration precision, we systematically merge some segmentation labels and feed the revised segmentations for training, leading to three modes: mode0 (foreground and background), mode1 (LV (LVBP+LVM), RV and background) and mode2 (LVBP, LVM, RV and background). In inference, we also introduce three distinct label configurations to evaluate the trained models, segmenting the original images into two (foreground+background), three (background+LV+RV), and four regions (background+LVBP+LVM+RV), as shown in Figure 8 (details in Appendix). The registration accuracy increases with a higher number of specified regions during inference, irrespective of the training labels. Interestingly, when comparing the outcomes of mode0, mode1, and mode2 using four regions

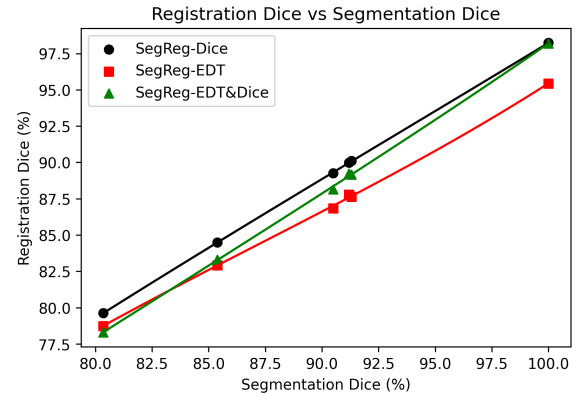


Figure 7: The registration performance of SegReg with the increasing segmentation accuracy.

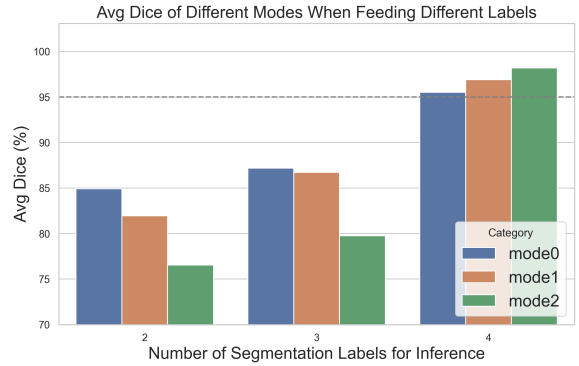


Figure 8: The registration accuracy of different modes when fed different numbers of labels as inputs.

(LVBP, LVM, RV, and background) as inputs, we observe no significant discrepancies, all exceeding 95% Dice. Hence, we conclude that within the SegReg framework, registration precision is predominantly determined by the number of regions defined for inference, rather than a strict correspondence between training and testing labels.

Conclusion

This work introduces a segmentation-enhanced registration framework, SegReg, which substantially surpasses current performance limits in both mono- and multi-modal registration. Unlike global smoothness constraints, SegReg predicts anatomically guided regional deformation fields via segmentation, preserving tissue boundary discontinuities. SegReg achieves near-perfect alignment (98.23% Dice) with GT segmentations while maintaining state-of-the-art performance even with automated segmentation inputs. Crucially, SegReg reveals a near-linear dependence of registration accuracy on segmentation quality, effectively transforming registration into a segmentation-driven process. Future iterations could replace the basic UNet backbone with more efficient backbones, and integrate foundation models like SAM to address segmentation challenges.

References

Ashburner, J. 2007. A fast diffeomorphic image registration algorithm. *Neuroimage*, 38(1): 95–113.

Avants, B. B.; Epstein, C. L.; Grossman, M.; and Gee, J. C. 2008. Symmetric diffeomorphic image registration with cross-correlation: evaluating automated labeling of elderly and neurodegenerative brain. *Medical image analysis*, 12(1): 26–41.

Avants, B. B.; Tustison, N. J.; Song, G.; Cook, P. A.; Klein, A.; and Gee, J. C. 2011. A Reproducible Evaluation of ANTs Similarity Metric Performance in Brain Image Registration. *Neuroimage*, 54(3): 2033–2044.

Balakrishnan, G.; Zhao, A.; Sabuncu, M. R.; Guttag, J.; and Dalca, A. V. 2018. An unsupervised learning model for deformable medical image registration. In *Proceedings of the IEEE conference on computer vision and pattern recognition*, 9252–9260.

Balakrishnan, G.; Zhao, A.; Sabuncu, M. R.; Guttag, J.; and Dalca, A. V. 2019. VoxelMorph: a learning framework for deformable medical image registration. *IEEE transactions on medical imaging*, 38(8): 1788–1800.

Beg, M. F.; Miller, M. I.; Trouvé, A.; and Younes, L. 2005. Computing large deformation metric mappings via geodesic flows of diffeomorphisms. *International journal of computer vision*, 61: 139–157.

Bernard, O.; Lalande, A.; Zotti, C.; Cervenansky, F.; Yang, X.; Heng, P.-A.; Cetin, I.; Lekadir, K.; Camara, O.; Ballester, M. A. G.; et al. 2018. Deep Learning Techniques for Automatic MRI Cardiac Multi-structures Segmentation and Diagnosis: Is the Problem Solved? *IEEE Transactions on Medical Imaging*, 37(11): 2514–2525.

Cao, X.; Yang, J.; Zhang, J.; Nie, D.; Kim, M.; Wang, Q.; and Shen, D. 2017. Deformable image registration based on similarity-steered CNN regression. In *Medical Image Computing and Computer Assisted Intervention- MICCAI 2017: 20th International Conference, Quebec City, QC, Canada, September 11-13, 2017, Proceedings, Part I* 20, 300–308. Springer.

Chen, C.; Miao, J.; Wu, D.; Zhong, A.; Yan, Z.; Kim, S.; Hu, J.; Liu, Z.; Sun, L.; Li, X.; et al. 2024a. Ma-sam: Modality-agnostic sam adaptation for 3d medical image segmentation. *Medical Image Analysis*, 98: 103310.

Chen, J.; Frey, E. C.; He, Y.; Segars, W. P.; Li, Y.; and Du, Y. 2022. Transmorph: Transformer for unsupervised medical image registration. *Medical image analysis*, 82: 102615.

Chen, X.; Diaz-Pinto, A.; Ravikumar, N.; and Frangi, A. F. 2021a. Deep learning in medical image registration. *Progress in Biomedical Engineering*, 3(1): 012003.

Chen, X.; Liu, M.; Wang, R.; Hu, R.; Liu, D.; Li, G.; and Zhang, H. 2024b. Spatially covariant image registration with text prompts. *IEEE Transactions on Neural Networks and Learning Systems*, 1–11.

Chen, X.; Xia, Y.; Ravikumar, N.; and Frangi, A. F. 2021b. A deep discontinuity-preserving image registration network. In *MICCAI*, 46–55. Springer.

Dalca, A. V.; Balakrishnan, G.; Guttag, J.; and Sabuncu, M. R. 2019. Unsupervised Learning of Probabilistic Diffeomorphic Registration for Images and Surfaces. *Medical Image Analysis*, 57: 226–236.

D’Antonoli, T. A.; Berger, L. K.; Indrakanti, A. K.; Vishwanathan, N.; Weiß, J.; Jung, M.; Berkarda, Z.; Rau, A.; Reisert, M.; Küstner, T.; et al. 2024. TotalSegmentator MRI: Sequence-Independent Segmentation of 59 Anatomical Structures in MR images. *arXiv preprint arXiv:2405.19492*.

Durrleman, S.; Prastawa, M.; Charon, N.; Korenberg, J. R.; Joshi, S.; Gerig, G.; and Trouvé, A. 2014. Morphometry of anatomical shape complexes with dense deformations and sparse parameters. *NeuroImage*, 101: 35–49.

Eppenhof, K. A.; and Pluim, J. P. 2018. Pulmonary CT registration through supervised learning with convolutional neural networks. *IEEE transactions on medical imaging*, 38(5): 1097–1105.

Fan, J.; Cao, X.; Yap, P.-T.; and Shen, D. 2019. BIRNet: Brain image registration using dual-supervised fully convolutional networks. *Medical image analysis*, 54: 193–206.

Hatamizadeh, A.; Nath, V.; Tang, Y.; Yang, D.; Roth, H.; and Xu, D. 2022. Swin UNETR: Swin Transformers for Semantic Segmentation of Brain Tumors in MRI Images. *arXiv preprint arXiv:2201.01266*.

Heinrich, M. P.; and Hansen, L. 2022. Voxelmorph++ going beyond the cranial vault with keypoint supervision and multi-channel instance optimisation. In *International Workshop on Biomedical Image Registration*, 85–95. Springer.

Heinrich, M. P.; Jenkinson, M.; Bhushan, M.; Matin, T.; Gleeson, F. V.; Brady, M.; and Schnabel, J. A. 2012. MIND: Modality independent neighbourhood descriptor for multi-modal deformable registration. *Medical image analysis*, 16(7): 1423–1435.

Heinrich, M. P.; Jenkinson, M.; Brady, M.; and Schnabel, J. A. 2013. MRF-Based Deformable Registration and Ventilation Estimation of Lung CT. *IEEE Transactions on Medical Imaging*, 32(7): 1239–1248.

Hering, A.; Häger, S.; Moltz, J.; Lessmann, N.; Heldmann, S.; and van Ginneken, B. 2021. CNN-based lung CT registration with multiple anatomical constraints. *Medical Image Analysis*, 72: 102139.

Hering, A.; Hansen, L.; Mok, T. C.; Chung, A. C.; Siebert, H.; Häger, S.; Lange, A.; Kuckertz, S.; Heldmann, S.; Shao, W.; et al. 2022. Learn2Reg: comprehensive multi-task medical image registration challenge, dataset and evaluation in the era of deep learning. *IEEE Transactions on Medical Imaging*, 42(3): 697–712.

Huang, Y.; Yang, X.; Liu, L.; Zhou, H.; Chang, A.; Zhou, X.; Chen, R.; Yu, J.; Chen, J.; Chen, C.; et al. 2024. Segment anything model for medical images? *Medical Image Analysis*, 92: 103061.

Hugo, G. D.; Weiss, E.; Sleeman, W. C.; Balik, S.; Keall, P. J.; Lu, J.; and Williamson, J. F. 2017. A longitudinal four-dimensional computed tomography and cone beam computed tomography dataset for image-guided radiation ther-

apy research in lung cancer. *Medical physics*, 44(2): 762–771.

Isensee, F.; Jaeger, P. F.; Kohl, S. A.; Petersen, J.; and Maier-Hein, K. H. 2021. nnU-Net: a self-configuring method for deep learning-based biomedical image segmentation. *Nature methods*, 18(2): 203–211.

Jena, R.; Sethi, D.; Chaudhari, P.; and Gee, J. C. 2024. Deep Learning in Medical Image Registration: Magic or Mirage? *arXiv preprint arXiv:2408.05839*.

Jia, X.; Bartlett, J.; Chen, W.; Song, S.; Zhang, T.; Cheng, X.; Lu, W.; Qiu, Z.; and Duan, J. 2023a. Fourier-net: Fast image registration with band-limited deformation. In *Proceedings of the AAAI Conference on Artificial Intelligence*, volume 37, 1015–1023.

Jia, X.; Bartlett, J.; Zhang, T.; Lu, W.; Qiu, Z.; and Duan, J. 2022. U-net vs transformer: Is u-net outdated in medical image registration? In *International Workshop on Machine Learning in Medical Imaging*, 151–160. Springer.

Jia, X.; Lu, W.; Cheng, X.; and Duan, J. 2024. Decoder-Only Image Registration. *arXiv preprint arXiv:2402.03585*.

Jia, X.; Thorley, A.; Gomez, A.; Lu, W.; Kotecha, D.; and Duan, J. 2023b. Fourier-Net+: Leveraging Band-Limited Representation for Efficient 3D Medical Image Registration. *arXiv preprint arXiv:2307.02997*.

Kang, M.; Hu, X.; Huang, W.; Scott, M. R.; and Reyes, M. 2022. Dual-stream pyramid registration network. *Medical image analysis*, 78: 102379.

Kirillov, A.; Mintun, E.; Ravi, N.; Mao, H.; Rolland, C.; Gustafson, L.; Xiao, T.; Whitehead, S.; Berg, A. C.; Lo, W.-Y.; et al. 2023. Segment anything. In *Proceedings of the IEEE/CVF International Conference on Computer Vision*, 4015–4026.

Li, Z.; Tian, L.; Mok, T. C.; Bai, X.; Wang, P.; Ge, J.; Zhou, J.; Lu, L.; Ye, X.; Yan, K.; et al. 2023. SAMConvex: Fast Discrete Optimization for CT Registration Using Self-supervised Anatomical Embedding and Correlation Pyramid. In *International Conference on Medical Image Computing and Computer-Assisted Intervention*, 559–569. Springer.

Marstal, K.; Berendsen, F.; Staring, M.; and Klein, S. 2016. SimpleElastix: A User-friendly, Multi-lingual Library for Medical Image Registration. In *Proceedings of the IEEE Conference on Computer Vision and Pattern Recognition Workshops*, 134–142.

Meng, M.; Feng, D.; Bi, L.; and Kim, J. 2024. Correlation-aware Coarse-to-fine MLPs for Deformable Medical Image Registration. In *Proceedings of the IEEE/CVF Conference on Computer Vision and Pattern Recognition*, 9645–9654.

Modat, M.; Ridgway, G. R.; Taylor, Z. A.; Lehmann, M.; Barnes, J.; Hawkes, D. J.; Fox, N. C.; and Ourselin, S. 2010. Fast free-form deformation using graphics processing units. *Computer methods and programs in biomedicine*, 98(3): 278–284.

Mok, T. C.; and Chung, A. 2020a. Fast symmetric diffeomorphic image registration with convolutional neural networks. In *Proceedings of the IEEE/CVF conference on computer vision and pattern recognition*, 4644–4653.

Mok, T. C.; and Chung, A. C. 2020b. Large deformation diffeomorphic image registration with laplacian pyramid networks. In *Medical Image Computing and Computer Assisted Intervention–MICCAI 2020: 23rd International Conference, Lima, Peru, October 4–8, 2020, Proceedings, Part III* 23, 211–221. Springer.

Mok, T. C.; and Chung, A. C. 2021. Large deformation image registration with anatomy-aware Laplacian pyramid networks. In *Segmentation, Classification, and Registration of Multi-modality Medical Imaging Data: MICCAI 2020 Challenges, ABCs 2020, L2R 2020, TN-SCUI 2020, Held in Conjunction with MICCAI 2020, Lima, Peru, October 4–8, 2020, Proceedings* 23, 61–67. Springer.

Ng, E.; and Ebrahimi, M. 2020. An unsupervised learning approach to discontinuity-preserving image registration. In *Biomedical Image Registration: 9th International Workshop, WBIR 2020, Portorož, Slovenia, December 1–2, 2020, Proceedings* 9, 153–162. Springer.

Rohé, M.-M.; Datar, M.; Heimann, T.; Sermesant, M.; and Pennec, X. 2017. SVF-Net: learning deformable image registration using shape matching. In *Medical Image Computing and Computer Assisted Intervention- MICCAI 2017: 20th International Conference, Quebec City, QC, Canada, September 11–13, 2017, Proceedings, Part I* 20, 266–274. Springer.

Shi, J.; He, Y.; Kong, Y.; Coatrieux, J.-L.; Shu, H.; Yang, G.; and Li, S. 2022. Xmorpher: Full transformer for deformable medical image registration via cross attention. In *International Conference on Medical Image Computing and Computer-Assisted Intervention*, 217–226. Springer.

Siebert, H.; Hansen, L.; and Heinrich, M. P. 2021. Fast 3D registration with accurate optimisation and little learning for Learn2Reg 2021. In *International Conference on Medical Image Computing and Computer-Assisted Intervention*, 174–179. Springer.

Tang, Y.; Yang, D.; Li, W.; Roth, H. R.; Landman, B.; Xu, D.; Nath, V.; and Hatamizadeh, A. 2022. Self-supervised pre-training of swin transformers for 3d medical image analysis. In *Proceedings of the IEEE/CVF Conference on Computer Vision and Pattern Recognition*, 20730–20740.

Vercauteren, T.; Pennec, X.; Perchant, A.; and Ayache, N. 2009. Diffeomorphic demons: Efficient non-parametric image registration. *NeuroImage*, 45(1): S61–S72.

Viergever, M. A.; Maintz, J. A.; Klein, S.; Murphy, K.; Staring, M.; and Pluim, J. P. 2016. A survey of medical image registration–under review.

Wang, H.; Ni, D.; and Wang, Y. 2024. Recursive Deformable Pyramid Network for Unsupervised Medical Image Registration. *IEEE Transactions on Medical Imaging*, 1–1.

Wang, J.; and Zhang, M. 2020. Deepflash: An efficient network for learning-based medical image registration. In *Proceedings of the IEEE/CVF conference on computer vision and pattern recognition*, 4444–4452.

Wasserthal, J.; Breit, H.-C.; Meyer, M. T.; Pradella, M.; Hinck, D.; Sauter, A. W.; Heye, T.; Boll, D. T.; Cyriac, J.;

Yang, S.; et al. 2023. TotalSegmentator: robust segmentation of 104 anatomic structures in CT images. *Radiology: Artificial Intelligence*, 5(5).

Xu, Z.; Lee, C. P.; Heinrich, M. P.; Modat, M.; Rueckert, D.; Ourselin, S.; Abramson, R. G.; and Landman, B. A. 2016. Evaluation of six registration methods for the human abdomen on clinically acquired CT. *IEEE Transactions on Biomedical Engineering*, 63(8): 1563–1572.

Yang, L.; Li, W.; Shu, Y.; Mi, J.; Huang, Y.; and Xiao, B. 2024. ShiftMorph: A Fast and Robust Convolutional Neural Network for 3D Deformable Medical Image Registration. In *Proceedings of the 32nd ACM International Conference on Multimedia*, 2814–2823.

Young, S. I.; Balbastre, Y.; Dalca, A. V.; Wells, W. M.; Iglesias, J. E.; and Fischl, B. 2022. SuperWarp: Supervised Learning and Warping on U-Net for Invariant Subvoxel-Precise Registration. In *International Workshop on Biomedical Image Registration*, 103–115. Springer.

Zhang, H.; Chen, X.; Hu, R.; Liu, D.; Li, G.; and Wang, R. 2024a. MemWarp: Discontinuity-Preserving Cardiac Registration with Memorized Anatomical Filters. In *International Conference on Medical Image Computing and Computer-Assisted Intervention*, 671–681. Springer.

Zhang, H.; Chen, X.; Wang, R.; Hu, R.; Liu, D.; and Li, G. 2024b. Slicer Networks. *arXiv preprint arXiv:2401.09833*.

Zhao, S.; Dong, Y.; Chang, E. I.; Xu, Y.; et al. 2019. Recursive cascaded networks for unsupervised medical image registration. In *Proceedings of the IEEE/CVF international conference on computer vision*, 10600–10610.

Appendix

A: Details of Registration in Abdomen Image. Compared with intra-subject registration, inter-subject registration is generally more challenging, due to the great variability and large deformations across subjects. We utilize a dataset of 30 abdominal CT scans (Xu et al. 2016) from the Learn2Reg challenge, each accompanied by segmentation masks for 13 anatomical structures. The dataset is divided into training, validation, and test sets, with 20, 3, and 7 scans, respectively, resulting in 380 (20×19) training pairs, 6 (3×2) validation pairs, and 42 (7×6) testing pairs. All images were resampled to a voxel resolution of 2 mm and standardized to a spatial size of $192 \times 160 \times 256$.

We utilize an online model Swin-UNETR (Tang et al. 2022; Hatamizadeh et al. 2022) to segment the abdomen images for our SegReg, available at <https://huggingface.co/darragh/swinunetr-btcv-base>. The registration results of SegReg when using segmentation as inputs are presented in Table A1. The distribution of results on abdomen registration is plotted in Figure A1, corresponding to the results in Table 2 and Table A1.

Model	Dice (%) \uparrow	HD95 (mm) \downarrow	SDlogJ \downarrow
Initial	30.86	29.77	-
SegReg-Dice(Ours)	68.02	20.77	0.58
SegReg-EDT (Ours)	67.19	21.04	0.52
SegReg-EDT&Dice (Ours)	67.74	21.73	0.60
SegReg-Dice (GT)	93.24	10.23	0.56
SegReg-EDT (GT)	92.09	9.62	0.48
SegReg-EDT&Dice (GT)	92.73	10.08	0.55

Table A1: Quantitative comparison between the registration performance of automatic segmentation and GT segmentation on the abdomen CT dataset.

B: Details of Registration on ACDC. We evaluate our SegReg in intra-subject cardiac MR image registration using the ACDC dataset (Bernard et al. 2018), with 80 subjects for training, 20 for validation, and 50 for testing. For each subject, the end-diastole (ED) and end-systole (ES) images have GT segmentations for LVBP, LVM and RV. We perform registration from both ED to ES and ES to ED, resulting in 160 training pairs, 40 validation pairs, and 100 test pairs. All images are pre-processed through resampling, normalization, cropping, and padding, into $128 \times 128 \times 16$ (spacing: $1.8 \times 1.8 \times 10 \text{ mm}^3$).

We utilize an online model nnUNet (Isensee et al. 2021) to segment the cardiac images for our SegReg, available at <https://zenodo.org/records/3734294>. The distribution of registration results on ACDC is presented in Figure A2, corresponding to the results in Table 1. In addition, the detailed results of Figure 7 are shown in Table A2. To obtain labels with varying segmentation, we train a nnUNetV2 from scratch, and then feed the results of different epochs (different accuracy) into SegReg, as noted in the table. The ‘nnUnetV1-online’ is the trained model we obtain directly online, without any fine-tuning, whose segmentation performance is only marginally lower than the best model trained by ourselves (“nnUnetV2-Best(997)”). Table A3 presents

the detailed results in Figure 8.

C: Details of Registration in ThoraxCBCT. To demonstrate the iterative registration performance of our SegReg framework, we conduct another intra-subject registration work using CT images from ThoraxCBCT (Hugo et al. 2017) in the Learn2Reg2023 challenge, where the registration is to register a planning fan-beam CT (FBCT) image into two cone-beam CT (CBCT) images at the beginning and end of therapy. The lack of paired data and the difference in image quality and resolution make it a challenging task. ThoraxCBCT contains three subjects for evaluation on the leaderboard. All the images are preprocessed by the challenge organiser to $390 \times 280 \times 300$ with a spacing of $1 \times 1 \times 1 \text{ mm}^3$.

To register the thorax images from ThoraxCBCT, all the testing data are segmented using <https://totalsegmentator.com/Totalsegmentator>. As there are a total of 117 segmentation labels and many of them are not correlated to the regions/organs on the thorax, we select and merge the segmentation labels into 13 classes, comprising aorta, inferior vena cava, lung, vertebrae and ribs, esophagus, trachea, pulmonary artery, left scapula, right scapula, left clavicular, right clavicular, heart and background.

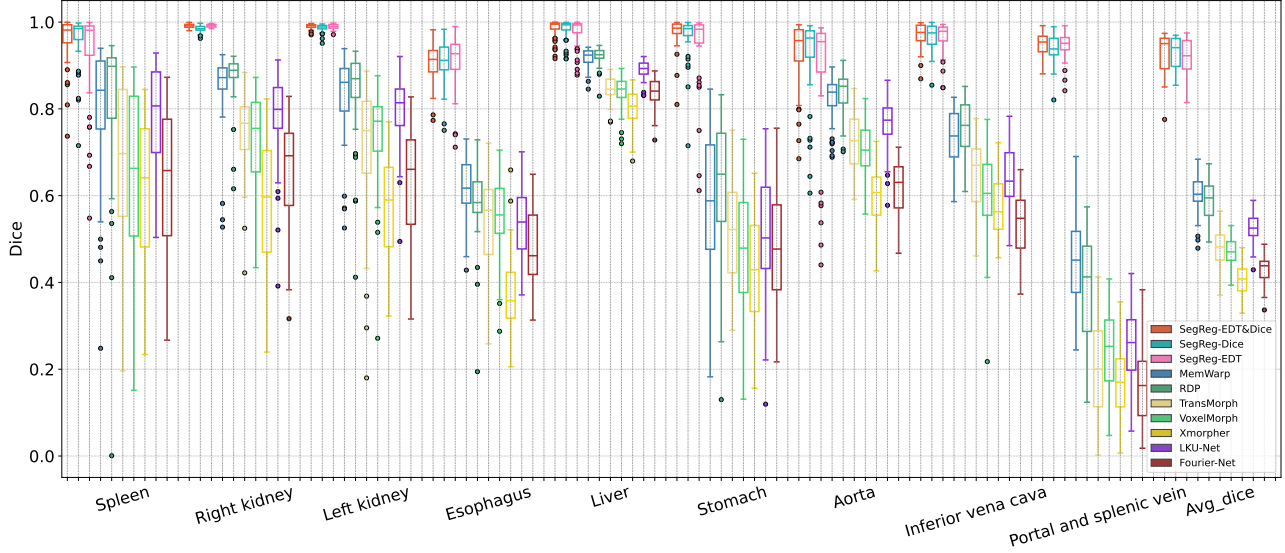


Figure A1: Boxplots on the abdomen CT dataset. SegReg-Dice, SegReg-EDT and SegReg-EDT&Dice achieve significantly higher Dice than the rest of the methods.

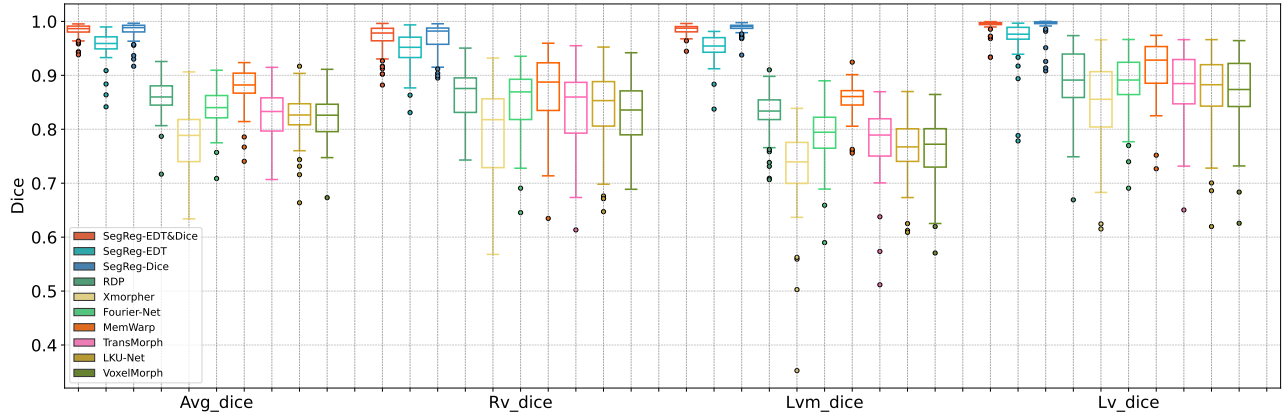


Figure A2: Boxplots on the ACDC dataset. SegReg-Dice, SegReg-EDT and SegReg-EDT&Dice achieve significantly higher Dice than the rest of the methods.

Model	Seg Dice (%) ↑	Avg. Dice (%) ↑	LV Dice (%) ↑	LVM Dice (%) ↑	RV Dice (%) ↑	HD95 (mm) ↓	SDlogJ ↓
Initial	58.14	61.60	48.33	64.50	11.95	-	-
SegReg-Dice (GT Seg)	100.00	98.23	99.15	98.74	96.81	1.93	0.36
SegReg-Dice (nnUnetV2-1)	80.35	79.62	84.77	76.15	77.94	8.84	0.37
SegReg-Dice (nnUnetV2-2)	85.38	84.49	89.09	80.88	83.52	6.91	0.31
SegReg-Dice (nnUnetV2-11)	90.50	89.27	92.92	87.25	87.62	5.19	0.34
SegReg-Dice (nnUnetV2-Best(997))	91.31	90.11	93.05	88.20	89.08	4.83	0.35
SegReg-Dice (nnUnetV1-online)	91.19	89.98	92.85	88.18	88.91	5.08	0.36
SegReg-EDT (GT Seg)	100.00	95.44	96.69	95.17	94.46	3.62	0.07
SegReg-EDT (nnUnetV2-1)	80.35	78.74	83.49	76.70	76.03	8.61	0.14
SegReg-EDT (nnUnetV2-2)	85.38	82.93	87.46	79.61	81.70	7.53	0.12
SegReg-EDT (nnUnetV2-11)	90.50	86.83	90.79	84.81	84.89	6.24	0.10
SegReg-EDT (nnUnetV2-Best(997))	91.31	87.64	90.92	85.32	86.69	5.95	0.08
SegReg-EDT (nnUnetV1-online)	91.19	87.79	90.89	85.67	86.81	6.03	0.09

Table A2: Registration performance of SegReg with the increasing segmentation on the cardiac ACDC dataset, where nnUnetV2-1, nnUnetV2-2, nnUnetV2-11 and nnUnetV2-Best(997) mean the segmentation are predicted using the trained nnUNet model at 1, 2, 11 and 997 epochs, respectively. Symbols indicate direction: ↑ for higher is better, ↓ for lower is better. “Initial” refers to baseline results before registration.

Model	Avg. Dice (%) \uparrow	LV Dice (%) \uparrow	LVM Dice (%) \uparrow	RV Dice (%) \uparrow	HD95 (mm) \downarrow	SDlogJ \downarrow
Initial	58.14	61.60	48.33	64.50	11.95	-
mode0 (background+foreground)	84.91	82.65	78.87	93.19	5.81	0.07
mode0 (background+LV+RV)	87.19	82.52	82.19	96.87	5.19	0.07
mode0 (background+LVBP+LVM+RV)	95.52	95.03	94.74	96.78	3.24	0.11
mode1 (background+foreground)	81.94	80.23	75.36	90.24	6.96	0.06
mode1 (background+LV+RV)	86.72	81.55	81.90	96.70	5.54	0.08
mode1 (background+LVBP+LVM+RV)	96.89	97.35	96.65	96.67	3.14	0.10
mode2 (background+foreground)	76.54	71.41	66.58	91.62	8.06	0.06
mode2 (background+LV+RV)	79.76	71.52	70.82	96.94	7.00	0.07
mode2 (background+LVBP+LVM+RV)	98.18	99.21	98.44	96.90	2.05	0.14

Table A3: Registration results of feeding different types of segmentation components into the SegReg framework. Symbols indicate direction: \uparrow for higher is better, \downarrow for lower is better. “Initial” refers to baseline results before registration.